SURFACE AND INTERFACE ANALYSIS, VOL. 8, 93-111 (1986)

REVIEW PAPER

The Relationship Between Electron and Ion Induced Secondary Electron Imaging: A Review With New Experimental Observations

S. Y. Lai, D. Briggs†, A. Brown and J. C. Vickerman
Department of Chemistry, UMIST, PO Box 88, Manchester, M60 1QD, UK
† ICI, Petrochemicals and Plastics Division, PO Box 90, Wilton, Middlesbrough, Cleveland, TS6 8JE, UK

The phenomenalogical and theoretical aspects of secondary electron emission due to ion bombardment in the keV energy range has been reviewed and a comparision of this process with secondary electron emission due to electron bombardment has been made. The similarities and differences between the contrasts in the secondary electron images of test specimens studied with both scanning microfocused Ga^+ beams and electron beams have been explained by the mechanisms of the secondary electron emission processes. From ion induced secondary electron images information on the topography, material and crystallographic nature of specimens can be obtained with high surface sensitivity. Differences in surface potential on different areas of a specimen has also been shown to result in voltage contrast effects.

INTRODUCTION

With the development of high brightness liquid metal ion sources, the use of scanning microfocus ion beams for secondary ion imaging (SIMS imaging) is becoming an important surface analytical technique giving compositional information with high spatial resolution.[1] On bombardment of the specimen surface with a high energy ion beam, as well as secondary ions, a high yield of secondary electrons is obtained. These secondary electrons can also be collected to obtain high resolution secondary electron images in a manner analogous to scanning electron microscopy. It is therefore very desirable for the mechanisms responsible for creating the secondary electron image contrast to be understood so that maximum information concerning the specimen may be obtained. The proper interpretation of secondary electron images requires an understanding of the process of interaction between a primary ion beam and a solid target leading to the electron emission. This paper attempts to review the phenomenon of ion-bombardment induced secondary electron emission and discusses the types of image contrast which are the characteristic of electron emission. Since SIMS imaging is performed with typically singly charged monatomic ion beams of up to a few tens of keV energy, the discussion will concentrate on processes occurring with this type of ions in this energy range although brief mention of the ion solid interaction in other energy ranges will also be made.

Ion induced secondary electron emission itself is an old subject of investigation as it is important in causing radiation damage by high energy particles, in the design of ion-electron converters for mass spectrometry and many other processes. Unfortunately, clean target conditions were not often achieved in the earlier experiments. The older literature has been covered by some excellent reviews (e.g. Refs 2-5). Here, emphasis will be placed on more recent investigations with clean targets under ultra-high vacuum conditions which give results more characteristic of the ion-target systems involved. The behaviour of metals, semiconductors and insulators will all be discussed. However, since the bombardment of insulators with ion beams leads to charging problems which affect the measurement of electron emission this area is less well studied. Information on ion-insulator systems is scanty compared with that on metals.

POTENTIAL ELECTRON EMISSION ON ION BOMBARDMENT

Two different types of electron emission processes can be distinguished—potential emission and kinetic emission. As an ion approaches a solid surface, neutralization of the ion may occur by the transfer of an electron from the target to the ion either by direct Auger neutralization or by resonance neutralization followed by Auger de-excitation of the excited state of the atom to the ground state. In both cases, the potential energy of the primary ion is converted into kinetic energy of a target electron. If the energy transfer is sufficient, the electron may be emitted from the target surface.[6,7] For a metal target, the maximum energy that can be transferred is E_i-ϕ, where E_i is the first ionization energy of the primary ion and ϕ is the work function of the target. The condition for potential emission to take place is therefore that E_i-$2\phi > 0$. From this consideration, potential electron emission will only be significant for positive ions of inert gases and electronegative elements, which possess high ionization energies. For bombardment of most metals by ions such as Cs^+ and Ga^+, potential electron emission will be absent. Furthermore, the coefficient of potential electron emission to a first approximation is independent of the energy of the primary ion and is typically rather smaller than unity

0142-2421/86/030093-19 $09.50

Received 28 October 1985
Accepted 10 December 1985

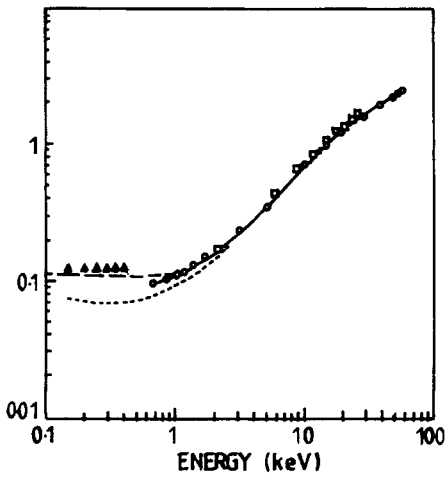

Figure 1. Secondary electron yield of Mo under Ar^+ impact versus projectile energy. The yield at projectile energy below 1 keV represent the yield due to potential emission. (Reproduced from Ref. 18 with the permission from the authors and the publisher).

(c.f. data quoted in Ref. 8). Therefore, at primary ion energies in the keV range, the contribution of potential emission to the total secondary electron yield will be small compared with kinetic electron emission although its effect is often not negligible for noble gas ion bombardment (Fig. 1).

KINETIC ELECTRON EMISSION BY ION BOMBARDMENT

Kinetic electron emission results from the transfer of the kinetic energy of a bombarding ion to the electrons

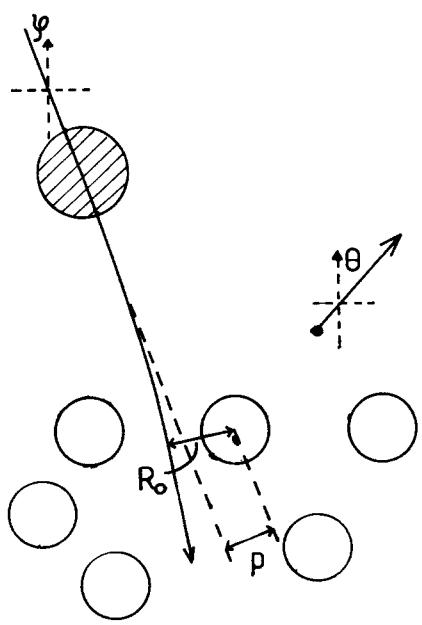

Figure 2. Definition of some terms used in the text to describe the projectile–target collision and the secondary electron emission processes. ⊜, Projectile ion; ○, target atoms; ●, secondary electrons; p, collision impact parameter; R_0, distance of closest approach of the colliding particles; φ, angle of incidence of the primary beam; θ, polar angle of secondary electron emission; →, direction normal to the target surface.

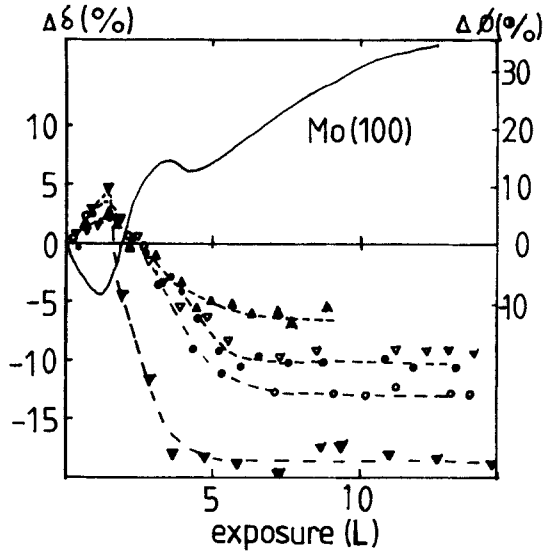

Figure 3. The change of secondary electron yield for Ar^+ bombardment of molydenum induce by oxygen exposure at 5×10^{-8} torr. The impact energies are: (▼) 5 keV, (○) 30 keV, (●) 40 keV, (▽) 50 keV, (▲) 60 keV. The full line is the change in work function. (Reproduced from Ref. 10 with the permission of the authors and the publisher).

of a projectile–target system as it slows down inside the target material. Studies have revealed certain characteristics of the process which will now be discussed. Some of the terms used in the discussion are defined in Fig. 2. Symbols which occur repeatedly in the text have been defined in the appendix. Others are defined where they appear in the text.

Effects of the target surface condition

The emission of secondary electrons is sensitive to the condition of the target surface. It has repeatedly been observed that metals contaminated by adsorbed gases have a greater secondary electron yield than that of the corresponding clean surfaces.[2–5,8] Part of the effect of surface adsorbates is caused by the change in work function of the metal on adsorption, which alters the escape probability of electrons liberated inside the target (Fig. 3). For example, hydrogen and oxygen adsorbed on molybdenum reduce the coefficient of secondary electron emission while potassium increases it.[9,10] The work function change alone is not sufficient to account for all the effects of the adsorbates, especially when the coverage is high. A contribution to the total yield by electron emission from adsorbed oxygen was proposed to account for the large increase in secondary yield when oxygen is adsorbed on aluminium.[10] Similarly, on contaminated insulator surfaces, the secondary electron yield was found to change on prolonged primary ion bombardment, presumably due to the cleaning of the target by ion sputtering.[11]

Energy dependence of the secondary electron yield

At very low primary ion energy, kinetic electron emission does not take place. A velocity threshold of the order of $0.6-2 \times 10^7$ cm s^{-1} (ca. 0.7–8 keV for Ar^+) for metal targets and a lower value for insulators is usually

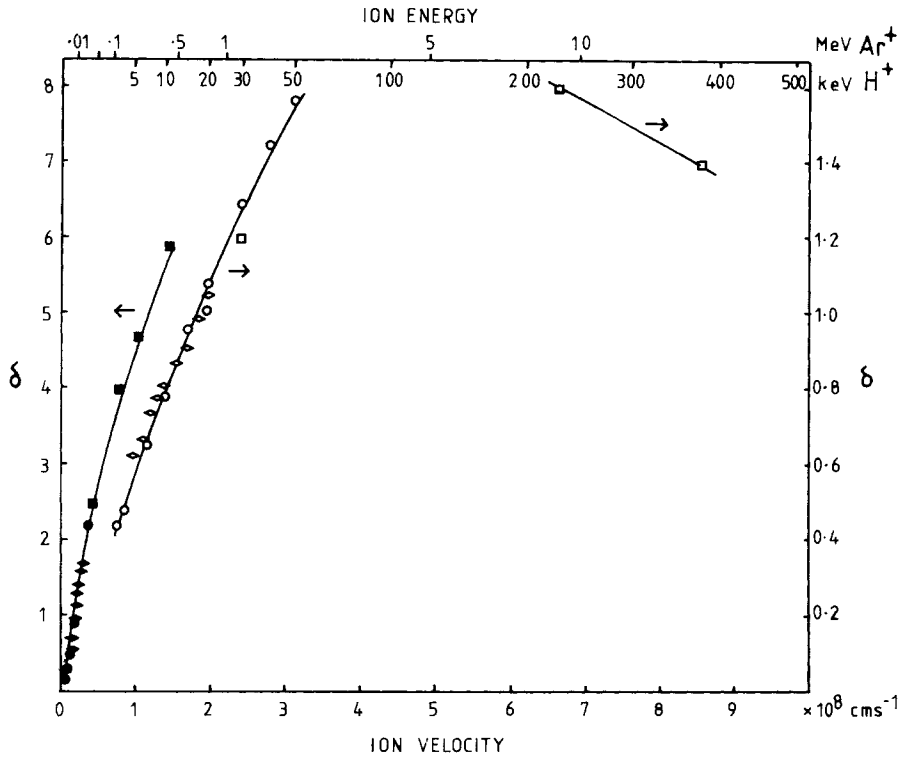

Figure 4. Secondary electron yields for H^+ and Ar^+ bombardment of polycrystalline copper as a function of the primary ion velocity. Ar^+, ● Baragiola *et al.*, ◆ Zalm and Becker, ■Svensson *et al.*; H^+, ○ Baragiola *et al.*, ◇ Zalm and Becker, □ Svensson *et al.*

required.[2] Above the threshold, the coefficient of electron emission increases first linearly with the ion energy and then linearly with the ion velocity. At higher energies, the value of which depends on the primary ion (it is of the order of a few hundred keV for H^+), the electron yield levels off and then decreases with further energy increase. Recent measurements on clean metal surfaces confirms the linearity of electron yield with ion velocity for most ions at the energy range of interest to SIMS imaging.[12-19] Data for secondary electron yield from polycrystalline copper by H^+ and Ar^+ bombardment taken from Ref 18, 19 and 20 is shown in Fig. 4.

Variation of secondary electron yield with the atomic number of the projectile

When the same target is bombarded with different primary ions at the same energy, the secondary electron yield in general falls with the increasing atomic number of the primary ion.[8,21,22] However, when compared at the same ion velocity, the data compiled by Fehn[22] for gas covered metal surfaces showed an increase of yield with increasing ion atomic number in a manner similar to the electron stopping power of the ions as predicted by the theory of Parilis and Kishinevskii (see fifth section). Superimposed on this trend an oscillation of the yield is observed which is related with the electronic structure of the primary ion. A comprehensive study by Thum and Hofer in which clean gold surfaces under UHV conditions were bombarded with ions having atomic numbers ranging from 3 to 92 showed an even more pronounced oscillation of secondary electron yield as a function of the electronic structure of the projectile ions[23] (Fig. 5).

Variation of secondary electron yield with the nature of the target material

The coefficient of secondary electron emission on some clean metal targets with 10 keV H^+ and Ar^+ taken from the publications by Baragiola *et al.*[8,16,18] and Zalm and Becker[19] are plotted as a function of the atomic number of the target in Fig. 6. Obviously, the number of target materials studied is not sufficient for any correlation of the electron yield with the electronic structure of the target to be made. The relative electron yields from

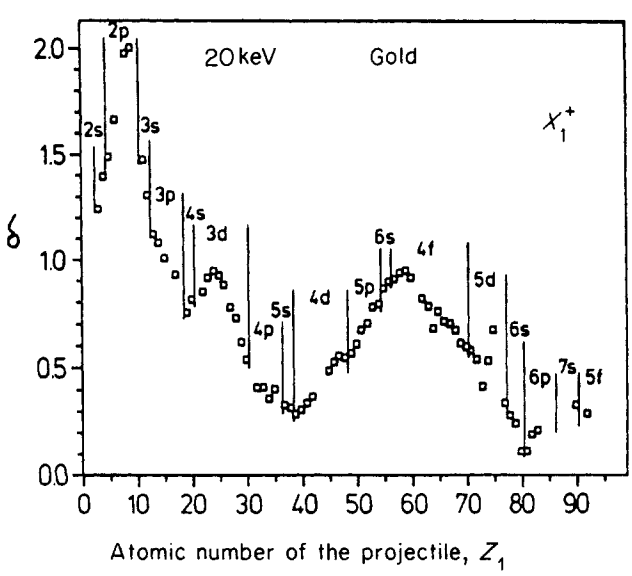

Figure 5. Variation of the electron yields by 20 keV impact of atomic ions on polycrystalline gold. (Reproduced from Ref. 23 with the permission of the authors and the publisher).

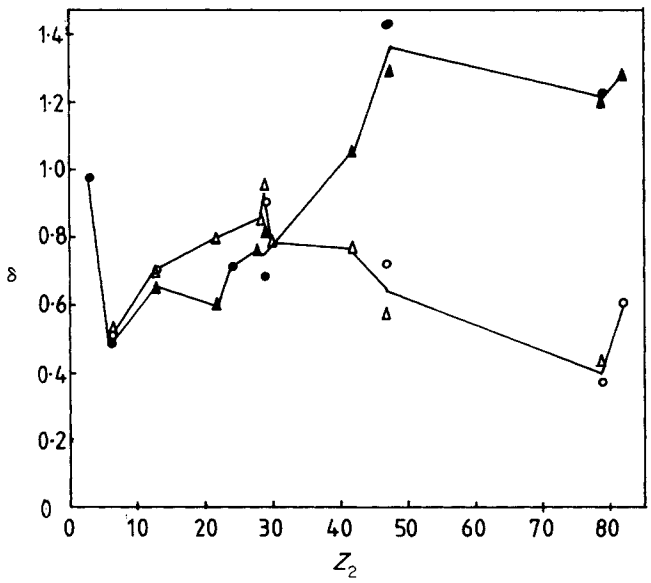

Figure 6. Variation of secondary electron yields by 10 keV H^+ and Ar^+ bombardment of some polycrystalline metals as a function of the atomic number of the targets. The open symbols are for Ar^+ bombardment and the filled symbols for H^+ bombardment. The data published by Baragiola *et al.* are denoted by circles and those by Zalm and Becker are denoted by triangles.

different materials depend to some extent on the energy at which the comparison is made and also on the nature of the projectile.

When positive ion bombardment of insulators is studied, sample charging often prevents the emission of secondary electrons. When this can be overcome, for example by using short ion pulses,[3] the secondary electron yield from insulators is found to be much higher than that from clean metal surfaces. (This accounts also for the high electron yield from metal surfaces covered with a thick layer of adsorbates.) The inelastic mean free path of secondary electrons within insulators is much larger than that within metals.[24] The absence of electrons in the conduction band, which can interact effectively with secondary electrons, causes much less attenuation of the secondary electron emission by an insulator compared with a metal.

Energy distribution of the secondary electrons

The most prominent feature of the energy spectra of secondary electrons emitted from metals on ion bombardment is a cascade peak whose intensity maximum typically lies below 10 eV energy. Peaks with specific energy due to processes like Auger de-excitation and plasmon de-excitation can be observed but are much less intense compared with the cascade peak[25,26] (Fig. 7(a)). Within a large energy range the position of the intensity maximum does not change with the energy of the primary ion beam (Fig. 7(b)). On molydenum the position of the peak changes only very slightly when bombarded with different ions.[27]

Angular distribution of the secondary electrons

The yields of secondary electrons emitted from polycrystalline metals as a function of the polar angle of emission

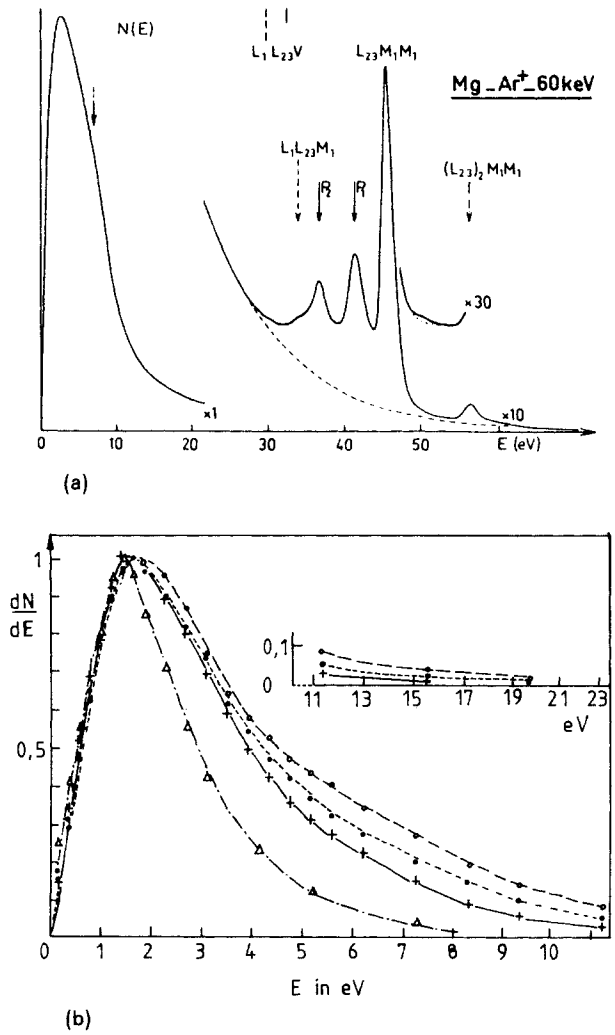

Figure 7. (a) Energy spectrum of the secondary electron emitted by Ar^+ bombardment of magnesium. (Reproduced from Ref. 25 with the permission of the authors and the publisher); (b) Energy distribution of the electrons emitted by the bombardment of Ar^+ on molydenum. Ion energy: (△) 2 keV, (+) 5 keV, (●) 10 keV, (○) 15 keV. (Reproduced from Ref. 27 with the permission of the authors and the publisher).

follows approximately a cosine distribution[28,29] (Fig. 8), suggesting that the distribution of the emitted electrons is isotropic within the target.

Dependence of the secondary electron yield with the angle of incidence of the primary beam

For polycrystalline or amorphous metals, semiconductors as well as insulators, the yield of secondary electrons increases with increasing angle between the primary beam and the target surface normal up to about 70°–80° [12,20,30-33] To a first approximation, the dependence of secondary electron yield with the angle of incidence of the primary beam can be described by a secant function. Secondary electrons released can only escape from a shallow depth within the target (typically about a few nm for metals and a few tens of nm for insulators.[24,34] If the primary beam retains the ability to excite secondary electrons after penetrating the target for a distance which is significantly larger than the electron escape distance then ignoring the possible effects of primary

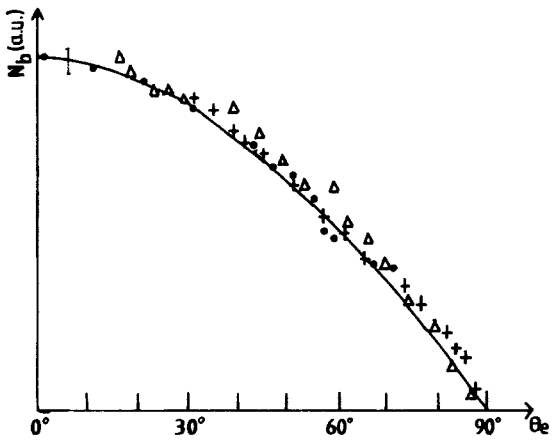

Figure 8. Polar angular distribution of secondary electron emission by Ar^+ bombardment of polycrystalline aluminium at different angle of incidence. (+) $\varphi = 0°$, (△) $\varphi = 15°$, (○) $\varphi = 30°$. The solid line indicates the cosine distribution. (Reproduced from Ref. 29 with the permission of the authors and the publisher).

ion scattering the path length of the primary beam within the secondary electron escape depth is a secant function of the angle of incidence and the secondary electron yield increases accordingly.

Deviations from the secant function however have been observed.[20,30] The increase of electron yield with the angle of incidence is smaller than predicted for Ar^+ bombardment of gold.[30] With heavy targets the primary ion velocity decreases within the secondary electron escape depth and so the increase in ion path length does not result in a proportionate increase in secondary electron yield. In the same paper, the yield from a boron target was also reported to show a smaller increase with the angle of incidence. Excitation of a surface state was proposed. When a medium or light target is bombarded by heavy ions, larger increases in secondary electron yield with the angle of incidence were observed[20] (Fig. 9). A contribution from recoil target atoms was suggested as the cause of this deviation.

Effect of the charge of the projectile

When comparison is made between the secondary electron yield from metals by the bombardment of ions of the same element with different electronic charge at the same velocity, it is often found that the yield is higher for ions with higher positive charge (for examples, between Ar^{2+}, Ar^+ and Ar^0; Ne^+ and Ne^0; O^- and O^+; Cl^- and Cl^+).[13,14] The difference can usually be explained by the contribution of potential emission to the total yield. The kinetic contribution was found to be independent of the ionic charges (Fig. 10). This is expected since the process of Auger neutralization essentially means that the ions are neutralized before striking the target surface. In the case of H^- bombardment, the secondary electron yield is higher than H^+ bombardment due to the detachment of electrons from the negatively charged ions.

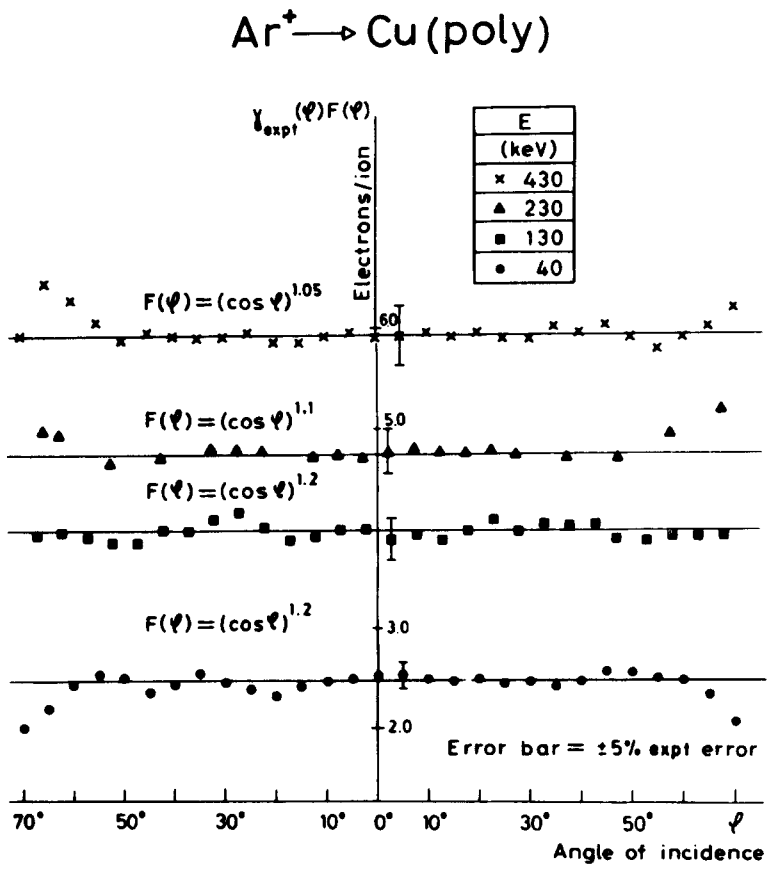

Figure 9. Dependence of the secondary electron yield on the angle of incidence for the bombardment of polycrystalline copper by argon ions. (Reproduced from Ref. 20 with the permission from the authors and the publisher).

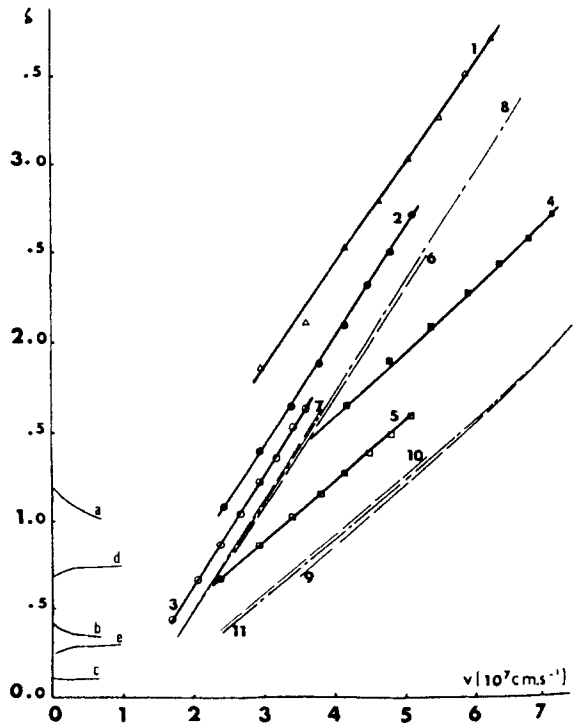

Figure 10. Variation of the coefficients of secondary electron emission as a function of the incident ion energy. δ_{exp}: 1-Ar^{3+}, 2-Ar^{2+}, 3-Ar^{+}, 4-Ne^{2+}, 5-Ne^{+}, δ_{kin}: 6-Ar^{2+}, 7-Ar^{+}, 8-Ar^{0}, 9-Ne^{2+}, 10-Ne^{+}, 11-Ne^{0}, δ_{pot}: a-Ar^{3+}, b-Ar^{2+}, c-Ar^{+}, d-Ne^{2+}, e-Ne^{+}, (Reproduced from Ref. 13 with the permission from the authors and the publisher).

Effect of the crystallographic structure of the target

When single crystal targets are bombarded with ions, the secondary electron yield varies with the orientation of the crystal lattice of the target with respect to the direction of the incoming beam. Normal incidence of ion beams on surfaces with more closely packed structure produced higher electron emission compared with surfaces with more open structure[35] (Fig. 11). Similarly, when the angle of incidence of an ion beam on a single crystal target is varied, minima in the secondary electron yield corresponding to incidence along low index directions were observed.[36,37] The magnitude of the crystallographic effect decreases with increasing temperature.[36]

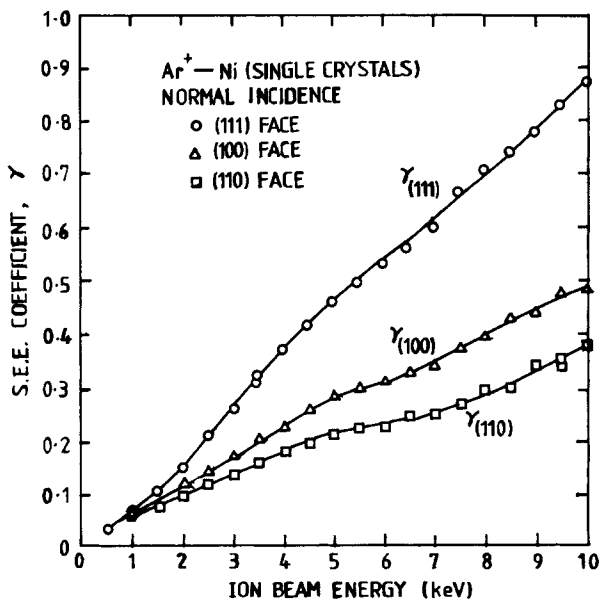

Figure 11. Secondary electron emission coefficient for Ar^{+} ions incident on the three low-index planes of nickel as a function of ion energy. (Reproduced from Ref. 35 with the permission of the authors and the publisher).

INELASTIC ENERGY LOSS OF IONS ON THE BOMBARDMENT OF A SOLID TARGET

Most theoretical discussions of the energy loss processes of ion-solid collision treat the target as simply a collection of atomic particles and the collision as binary collisions between a projectile ion and a target atom, with the neighbouring atoms in the solid lattice playing a negligible role.[4,5,38,39] At primary ion velocities much below v_0, elastic energy loss predominates while at the other extreme, when $u \gg v_0$, inelastic processes become more important.

At high primary ion energy, $u > v_0$, Bohr[40] considered an ion-electron collision as a free collision in a Coulomb field. Using a classical analogy of the Bethe's theory,[41] the average energy transfer in each ion-atom collision was determined to be:

$$T_{av} = \frac{4\pi Z_1^2 e^4 Z_2}{mu^2} \ln\left(\frac{2mu^2}{I_e}\right) \tag{1}$$

where I_e is the average excitation energy of the target electrons.

The electron stopping power of an ion-target combination is:

$$\frac{-dE}{dx} = \frac{2\pi N e^4 Z_1^2 Z_2}{mu^2} \ln\left(\frac{2mu^2}{I_e}\right) \tag{2}$$

The maximum energy that can be transferred in the direct ion-electron collision model is

$$T_m = \frac{4m}{M_1} E_0 \tag{3}$$

Because of the large mass mismatch between an ion and an electron, this energy transfer process is ineffective in electron excitation at low primary ion energy. Alternative processes have been proposed by Firsov[42] and Linhard and coworkers.[38]

Firsov's model was first proposed to describe the interaction between atoms taking part in collisions in the gaseous phase.[41] When a moving atom approaches a stationary one, the electron clouds overlap. The electrons from each atom come under the influence of the potential field of the other atom and energy is lost to the electrons in a 'frictional' type of process. The energy transfer depends on the impact parameter of the collision. The average energy loss for an ion penetrating a target obtained by integrating over all possible impact parameters is:[39]

$$\frac{-dE}{dx} = 2.34 \times 10^{-21} N(Z_1 + Z_2) E^{1/2} \text{ eV/m} \tag{4}$$

Linhard and coworkers however treat the ion-target interaction as between the moving ion and a sea of electrons which results in both collective plasmon excitation and direct electron excitation by ion-electron collision.[38] Similar to Firsov, the inelastic energy loss of the ion was found to be directly proportional to the ion velocity when the velocity of the primary ion beam is less than $Z_1^{2/3}v_0$.

THEORIES OF KINETIC ELECTRON EMISSION

Many theoretical models have been advanced to account for the kinetic emission of secondary electrons by ion bombardment. A critical discussion of some of them have been given in Refs 2 to 5 and more recently in Ref. 8. Here, only those that are more often invoked in the modern literature are discussed.

The theory of Parilis and Kishinevskii[43–45]

These authors consider the emission of secondary electrons on bombarding metal targets with 1 to 100 keV ions. The process of secondary electron emission was separated into 3 stages: electron excitation by ion-target interaction; secondary electron formation via Auger de-excitation and electron transport from the interior of the target to the vacuum.

Firsov's model was used to describe the ion-target interaction and it was assumed that energy transfer occurs between the projectile ions and the bound electrons of the metal atoms. Using the Thomas-Fermi model for the electron distribution, the inelastic energy transfer at impact parameter p is:

$$T(p) = \frac{\hbar u_0}{\pi a_0^2}(Z_1+Z_2)^2 \int_{R_0}^{0} \frac{[1-V(R)/E]\mathrm{d}R}{\sqrt{1-V(R)/E\text{-}p^2/R^2}} \times \int_{R/2}^{\infty} \frac{\chi^2(\rho)\,\mathrm{d}\rho}{\rho} \quad (5)$$

where $V(R)$ is the potential of repulsion between the projectile and target atoms at a distance of separation R and $\chi(\rho)$ is the Thomas-Fermi screening function. Considering the possibility of exciting more than one electron at each collision, the cross section for core level excitation is

$$\sigma = 2\pi \int_0^{p_1} \frac{T(p)}{J} p\,dp \quad (6)$$

Where p_1 is the impact parameter at which the energy transfer is

$$T(p_1) = E_b - \phi,$$

the minimum energy required for the excitation of an electron from a band of energy E_b to the conduction band. In the case of $1/4 < Z_1/Z_2 < 4$, (6) can be expressed as[43]

$$\sigma(u_0) = \frac{1.39 a_0 \hbar}{J}\left(\frac{Z_1+Z_2}{\sqrt{Z_1}+\sqrt{Z_2}}\right)^2 S(u_0) \quad (7)$$

where $S(u_0)$ is a complex expression, which may be approximated by

$$S(u_0) = 5.25u_0 \arctan 0.6\times 10^{-7}(u_0 - u_{\min}) \quad (8)$$

where $u_{\min}$ is the threshold velocity for secondary electron emission. A further assumption is made that the directly excited electrons have insufficient energy to surmount the potential barrier and remain bound. Electron emission is effected by Auger recombination of an electron from the conduction band to the core hole, with the simultaneous ejection of another conduction electron into the vacuum. The probability of such a process is given by the empirical relation

$$\omega(E_b) = 0.016(E_b - 2\phi) \quad (9)$$

A diffusion-absorption model was used to describe the process of secondary electron transport from within the target. The probability of an electron reaching the target surface decreases exponentially with the depth at which it is formed. The total secondary electron yield is therefore

$$\delta = \int_0^{x_m} \sigma(u)\omega(E_b) N e^{-x/L}\,\mathrm{d}x \quad (10)$$

where x_m is the maximum depth at which the velocity of the primary ion still retains the ability to produce secondary electrons. The velocity decrease of the primary ions inside the target was estimated by assuming that elastic energy loss predominate in the energy range. The secondary electron yield is then given by

$$\delta = N\omega(E_b)L[\sigma(u_0) - \Delta\sigma(u_0)] \quad (11)$$

$\Delta\sigma(u_0)$ accounts for the loss of velocity of the primary beam within the secondary electron escape depth in the target. At high primary velocity, when the velocity of the primary ion is approximately constant over the region of the secondary electron escape depth, the term $\Delta\sigma(u_0)$ can be ignored. The linear relationship between the secondary electron yield and the ion velocity well above threshold is thus predicted. This theory was later extended to ion-target pairs of other mass ratios[44] and to take into account the effects of recoil target atoms.[45]

The single collision theory of Harrison, Carlston and Magnuson[46]

According to the model of Parilis and Kishinevskii, the maximum energy of the secondary electrons is $E_b - 2\phi$. While most secondary electrons emitted are of energies lower than 10 eV, the maximum energy of the electrons at moderate primary energies exceeds that predicted by the Auger process. In contrast to the theory of Parilis and Kishinevskii, Harrison *et al.* proposed a process of direct electron excitation.[46] The inelastic energy transferred on ion-target collision was also estimated using the Firsov model. In contrast to Parilis and Kishinevskii, who considered only the excitation of the bound electrons of the target atoms, the authors pointed out that the kinetic energy of the projectile ion is distributed between the electron clouds of both the projectile and target and so excitation of the projectile ions is possible. Consequently the effect of the electronic structure of the projectile ions on the secondary electron yield cannot

be ignored. In this model, only the first collision between the projectile and target atoms were considered effective in electron excitation. The variation of the secondary electron yields with the crystallographic structure of the targets was correctly reproduced. However, such a single collision model is at variance with the idea that kinetic secondary electron emission is a bulk process.

The formulation of Baragiola *et al.*[8,18]

The experimental results obtained by Baragiola *et al.* indicated that the cross section for inner shell excitation of the target and the secondary electron yield have very different dependence on the energy of the primary beam and that the threshold for secondary electron emission by Ar^+ bombardment of clean Mo calculated by the theory of Parilis and Kishinevskii using the correct energy of the 4p level for Mo was actually much higher than that experimentally found.[18] Direct excitation of the valence electrons was considered important in secondary electron generation. The physical process effecting ionization however depends on the nature of the ion-target pair. For light ions bombarding free-electron metals, direct binary collision between the ion and the free electrons is important. In the case of heavy ions, the threshold is lower than that predicted by the binary ion-electron collision process. Inelastic energy transfer in Firsov's model in which all electrons of the target atom including the valence electrons take part was assumed. As the Z_1 dependence and energy dependence of the secondary electron yield follows the electron stopping power reasonably well, the authors proposed the use of a semi-empirical formula to describe the secondary electron emission process:

$$\delta = \frac{p}{2J}\int_0^\infty S_e(u, x)\exp(-x/L)\,dx \qquad (12)$$

which can be simplified to

$$\delta = PLS_e(u_0)/2J \qquad (13)$$

at high primary energy.

The theory of Sternglass[47]

A similar semi-empirical theory for secondary electron emission at high primary energy, of the order of MeV for H^+ was proposed by Sternglass. The energy loss of the primary ion was estimated by the method of Bohr[40]

$$\frac{-dE}{dx} = \frac{2\pi Ne^4 Z_1^2}{E_{eq}}\Sigma_{n,l} Z_{n,l}\ln\left(\frac{4E_{eq}}{I_{n,l}}\right) \qquad (14)$$

where $E_{eq} = \frac{1}{2}mu^2$; $I_{n,l}$ is the binding energy of an electron in the n,l shell; $Z_{n,l}$ is the number of electrons in the n,l shell.

At lower energy when only the outermost shells participate in ionization, the equation can be approximated by

$$\frac{-dE}{dx} = 2\pi Ne^4 Z_1^2\left(\frac{4Z^{1/3}}{\sqrt{I_0 E_{eq}}}\right) \qquad (15)$$

I_0 is the Rydberg energy.

Two types of collisions were considered; close collisions which produce high velocity recoil electrons which in turn excite slow secondary electrons and distant collisions from which low energy secondary electrons are produced directly. As the momentum gained by the fast recoil electrons are directed towards the interior of the target, only part of the energy of these electrons are available for slow secondary electron production at the depth where they are produced. The rest of the energy is transported into deeper layers of the target. Using the equipartition rule suggested by Bohr,[40] the energy available for secondary electron production at depth x is

$$\left(\frac{dE}{dx}\right)_{close} f(u) + \left(\frac{dE}{dx}\right)_{distant} = \tfrac{1}{2}\left(\frac{dE}{dx}\right)_{total}[1+f(u)] \qquad (16)$$

$$\delta = \int_0^\infty \frac{1}{2J}\left(\frac{dE}{dx}\right)_{total}[1+f(u)]P_2^{\frac{1}{2}}\exp\left(\frac{-x}{L}\right)dx \qquad (17)$$

The decrease of secondary electron yield with increasing ion energy is predicted by the change of electron stopping power with ion energy in this energy range.

The cascade theory of secondary electron emission[48,49]

The division of the process of secondary electron emission into the stages of production and transportation is only a simplification of the real process. In fact the bombardment of a target with energetic ions sets up a cascade of ion-lattice atom, fast recoil-lattice atom and electron-electron collisions all of which can generate secondary electrons. The cascade process was treated by Schou for high energy ion as well as electron bombardment.[48,49] The cross-sections of the various collision processes were calculated on the assumption of a screened Coulomb potential between the interacting particles expressed in a power law. A system of transport equations was solved for the energy and angular distribution and the total yield of secondary electrons. Holmen *et al.* argued that the cascade process is still important for ion beams with energy in the keV range and the secondary electron yield depends on the energy deposited in electronic excitation at the target surface rather than on the ionization cross section.[50] The binary collision model is however not applicable and the secondary electron yield is more appropriately described by experimental stopping powers. In the cascade model, the secondary electron yield for normal ion incidence is:

$$\delta = \left[b_0 NS_e(E) + b_r NS_n(E)\frac{\eta_{(t)}(\gamma E)}{\gamma E}\right]\Lambda \qquad (18)$$

where Λ is a material parameter; The effects of the surface barrier and target-electron interactions are taken into account of by this constant, which is assumed to be approximately independent of the energy and nature of the primary beam; b_0 and b_r are constants accounting for the spatial distribution and transport of the elastic and inelastic energy to and from the target surface; $\eta_{(t)}(\gamma E)/(\gamma E)$ is the fraction of the energy transferred to the target atoms by elastic collision that end up in energy of electron excitation; $\gamma E = 4M_1M_2/(M_1+M_2)^2E'$ which is the maximum energy that can be transferred by elastic collision in an ion-target collision.

The angular and energy distribution of the emitted secondary electrons by both ion and electron bombardment are both well described by this theory.

While the cascade theory is conceptually a more realistic model for the electron excitation process, the parameters in the yield equation cannot be easily determined theoretically from the physical parameters of the ion-target system. This reflects the complexity of the process of secondary electron emission. The electron stopping power must take into account Auger and plasmon excitation-de-excitation processes. The energy deposited in the target surface region which is important for secondary electron emission can be strongly influenced by the scattering of the primary beam in the target. The extent to which these processes occur depends on the nature of the primary ion beam, the target properties and the energy of the ions.

Crystallographic effects in ion bombardment[51,52]

The above theories mostly deal with the ion bombardment of random targets. When the targets are crystalline, the electron yields also depend on the direction of the primary beam with respect to the crystallographic orientation of the targets. In their simple theory, Harrison *et al.* are able to explain the lower secondary electron yield obtained for ion bombardment on more open crystallographic planes relative to the more close-packed planes.[45] However, since electron emission is a bulk process, the trajectory of the ion beam within the target has to be considered. The crystallographic effect can be better explained by the phenomenon of ion channelling.[51,52] When an ion beam is directed nearly parallel to a low index crystallographic direction, ions that pass close to a row of atoms in the lattice suffer large angular deflections and the paths of these ions become randomized. Ions that pass further away from the atomic rows suffer only a series of correlated low impact parameter collisions that result in small angular deflections. For these ions, it is possible to describe them as experiencing an average potential of the entire row of atoms which is directed away from the strings of lattice atoms and so they are prevented from approaching close to them.[53,54] Such ions are described as 'channelled'. When the angle the beam makes with the crystallographic axis is larger than a critical value, all the ions enter the random beam and no channelling can be observed. Since both elastic and inelastic energy loss is impact parameter dependent, ion channelling has the effect of reducing the yield of secondary electrons as well as the sputtering yield.

COMPARISON BETWEEN ION-INDUCED AND ELECTRON-INDUCED SECONDARY ELECTRON EMISSION

A detailed review of electron induced secondary electron emission will not be attempted here. Interested readers are referred to reviews that already exist in the literature.[55-57] The following discussion aims only to point out the similarities and differences between the ion and electron induced processes in the keV energy range since this is the energy range relevant to both SIMS imaging and scanning electron microscopy.

There are many experimentally observed similarities between the two processes. Indeed as will be shown later, some of the empirical theories of ion induced emission are formulated by analogy with those of the electron induced processes and in the cascade theory of Schou,[48,49] a unified theory for the two processes was attempted.

The energy spectra of the secondary electrons are very similar for ion and electron bombardment except that for the electron induced case, there are peaks at energies near to that of the primary beam which correspond to backscattered primaries that have suffered large angular deflections by elastic scattering with only small or no energy loss.[57,58] The secondary electrons produced by electron bombardment follow nearly a cosine angular distribution[59] and the variation of secondary yield with the angle of incidence of the primary beam is approximately described by a secant function.[57] The secondary electron yields for both ion and electron bombardment are sensitive to the presence of surface contaminants. Yields from electron bombardment of insulators are much higher than those from metal targets.[60] As with ion bombardment, an electron beam hitting a solid target penetrates into the target and on its way losses energy to the target atoms by both elastic collisions with the target nuclei and inelastic collisions individually with target electrons or collectively with the Fermi sea. Electrons liberated by the inelastic processes interact with the target generating further secondary electrons and eventually become absorbed by the bulk or emitted through the surface of the target. Thus, except for a possible effect of a difference in the energy of the initially produced secondary electrons, the properties of the secondary electrons emitted which depend largely on the interactions of the generated secondaries with the targets, for example the energy, angular distribution of the secondary electrons and the effect of the surface conditions on the electron yield, should not be affected strongly by the nature of the primary species.

On the other hand, the dependence of secondary electron yield on the energy of the primary beam at the relevant energy range are different. While as in the case of the ion induced process, the secondary electron yield increases first with the primary energy and then decreases after reaching a maximum, the position of the energy maximum is at much lower energy, only a few hundred eV[60], compared to the several hundred keV for ion bombardment. The energy dependence of secondary electron yield for electron bombardment in the keV energy range is more similar to that for ion bombardment in the MeV energy range. One obvious difference between bombarding ions and electrons is their large difference in masses. For particles of the same velocity, the energy of an ion beam is more than a thousand times larger than that of an electron beam. Since the Bethe's theory for the inelastic energy loss of particle collisions is only applicable for projectile velocities large compared with the orbital velocities of the target electrons,[4] direct electron excitation by projectile-target electron collision is effective for electron probes of energies less than one keV but only effective for ion probes of much higher energies.

The small mass of the electrons have another consequence. Elastic collisions between electrons and the target nuclei only result in small energy transfers but large angular deflections of the primary beam. A large fraction of the primary beam is backscattered from the interior of the target. The coefficient of electron backscattering increases with increasing average atomic mass but not with the electronic structure of the target.[61,62] The backscattered electrons produce additional secondary electrons since energy that would otherwise have been lost to the target interior is returned to the surface region. This accounts for the general trend of increase in secondary electron yield with increasing atomic number for metals in the same group. In scanning electron microscopy, the backscattered electrons can be selectively measured for compositional analysis.

In the early elementary theories for secondary electron emission by electron bombardment,[63,64] the process of secondary electron emission was also divided into the steps of excitation, transport and emission and the yield estimated by the now familiar expression:

$$\delta = \frac{-P}{J}\int_0^\infty \frac{dE}{dx} e^{(-x/L)}\, dx \qquad (19)$$

The inelastic energy loss was taken as equivalent to the total energy loss of the electron beam and is estimated using the Thomson-Whiddington law for energy retardation:

$$E^2(x) = E_0^2 - 2Ax \qquad (20)$$

which predicts an inverse proportionality between the electron yield with the primary electron energy.

Experimentally, the secondary yield for primary electron beams in the keV energy range was found to decrease more slowly with the primary energy than would be predicted by (20).[55] Transmission experiments also showed that instead of an increasing energy loss of the primary electron beam with the depth inside the target as predicted by the Thomson-Whiddington law, the rate of energy loss is nearly constant with target depth, as a result of the scattering of the primary beam.[65,66] Better agreement with experimental results is obtained when the rate of energy loss is estimated by the use of the constant loss model, in which

$$-dE/dx = E_0/R \qquad (21)$$

and the range of the primary beam estimated using the power law:

$$\text{Range} = E_0^n/An \qquad (22)$$

with $n = 1.35$.

Energy loss expressions similar to the empirical expression were arrived at by Kanaya *et al.* using a screened Coulomb interaction model.[67] The value of n was allowed to increase with the energy of the primary beam and at high energy in the MeV range, n approaches 2, in agreement with the Thomson-Whiddington law.

THE CONTRAST MECHANISMS OF ION-INDUCED SECONDARY ELECTRON IMAGES

Scanning electron microscopy is a well established technique for material studies. The contrast mechanisms for secondary electron images are well known to the electron microscopists.[68,69] Since there are many similarities between the processes of secndary electron emission induced by energetic ions and electrons, it is instructive to compare the secondary electron images produced by ion bombardment and by electron bombardment and observe how far experience gained in scanning electron microscopy can be used for the interpretation of ion-induced secondary electron images. This has been pursued in the authors' laboratory.

The equipment used for ion-induced secondary electron imaging has been described in detail in Ref. 70. Test specimens were studied with a 5 or 10 keV Ga^+ beam produced by a Vacuum Generators MIG100 gallium liquid metal gun in an ultrahigh vacuum chamber. Scanning electron micrographs of the specimens were obtained with a Cambridge Stereoscan 150 scanning electron microscope or a Philips SEM 505 scanning electron microscope. In all three instruments the secondary electrons are detected using scintillator-photomultiplier units.

According to the convention of scanning electron microscopy, the contrast between two points A and B of an image of an object is defined as

$$C = \Delta S/S_{av} \quad \text{or} \quad C = 2|S_A - S_B|/|S_A + S_B| \qquad (23)$$

where S is the secondary electron signal measured at the image points A and B. The electron signal measured at any image point depends on the coefficient of secondary electron emission and on the fraction of the emitted electrons reaching the detector. Both the 'number' effect and 'trajectory' effect must be considered in the interpretation of image contrast.

Topographic contrast

When an irregular object is observed, different areas of the specimen may incline at different angles with respect to the primary beam of ions or electrons. Since the coefficient of secondary electron emission depends on the angle of incidence of the primary beam to the target surface, the number of secondary electrons emitted from the different areas will be different. If the efficiency of secondary electron collection is 100%, as is sometimes assumed for the scintillator-photomultiplier type of detector with positively biased detector front end, this number effect is the only source of topographic contrast. In practice, however, not all the electrons emitted are detected. Since the yield of secondary electrons is a maximum in the direction of the surface normal, the area of the specimen which faces the detector is more favourably disposed for secondary electron detection (Fig. 12). This is especially true for the electron induced images since in this case, the backscattered electrons too are detected. As the energy of these backscattered electrons are high, their trajectories are little affected by the detector front end potential and can only be detected when they are emitted towards the detector.

A stainless steel ball bearing of 1.5 mm diameter was used as a model specimen for the study of the gross topographic contrast. On a spherical object, all possible angles of incidence of the primary beam are represented. In the ideal case when all the secondary electrons are collected and the coefficient of secondary electron

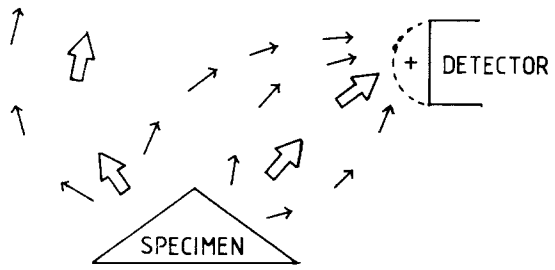

Figure 12 Trajectory effect in the detection of secondary electrons caused by the topography of the specimen.

emission follows the secant rule, the measured secondary electron intensity across a diameter of the sphere would be as shown in Fig. 13. The secondary electron image induced by 5 keV Ga^+ ion bombardment together with an intensity line scan across a line passing a diameter of the specimen in the plane of the detector is shown in Fig. 14(a). A qualitatively similar image was obtained by electron bombardment in the Cambridge Stereoscan 150 scanning electron microscope (Fig. 14(b)). The image brightness increases towards the edge of the sphere as predicted from the change in the angle of incidence. Quantitatively however, it is observed that the rate of increase of the secondary electron signal towards the edge of the specimen is less rapid for the Ga^+ induced image. This can be attributed to the smaller penetration depth of the Ga^+ beam. For heavy target materials and low energy primary ion beam, one may expect the number effect of topographic contrast to be less pronounced compared with those obtained by scanning electron microscopy.

At the same time, one observes that in both images, the signal intensity across the specimen is asymmetrical, with the side facing the detector appearing brighter, a vivid illustration of the trajectory effect. Although the ion induced image includes no high energy backscattered electrons, the trajectory effect is still important since in the SIMS imaging equipment, apart from the Ga^+ ion source, a quadrupole mass spectrometer and other ions sources are placed close to the specimen and the secondary electrons emitted in a direction away from the secondary electron detector are likely to be intercepted by these instruments. The trajectory effect is an instrument dependent phenomenon. The secondary electron image of the same sphere obtained using the Philips SEM 505 scanning electron microscope is shown in Fig. 14(c) for comparison. The asymmetry in the image is much less evident since the angle subtended by the detector in this instrument is much larger than that for the SIMS imaging instrument and the Cambridge Stereoscan 150 scanning electron microscope and so the emitted electrons are more effectively collected.

Another source of topographic contrast is the phenomenon of specimen absorption. On a highly irregular object, secondary electrons emitted from points which are sheltered from the detector by adjacent parts of the specimen may be absorbed by the specimen and so cannot be detected. To study this effect, a polished zinc-tin alloy with 20% zinc deeply etched with dilute HCl was examined. (The preparation of the alloy will be given in more detail in the next section) The alloy is composed of a zinc-rich phase in the form of elongated strands embedded in a tin-rich matrix. When the zinc-

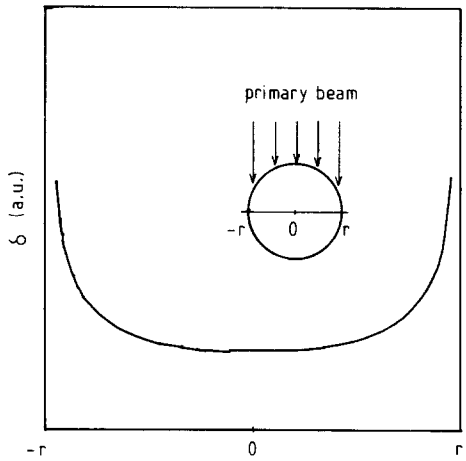

Figure 13. Theoretical intensity of secondary electron emission across a diameter of a spherical object. The inset shows the idealized geometry of the bombardment.

rich phase was dissolved away by the action of the acid, hollows with different diameters are left on the specimen surface. In both the ion and electron induced secondary electron images (Fig. 15), the 50 μm wide hollows (A) showed a gradation of brightness as the angle of incidence of the primary beam changed. The tiny hollows that are about 1 to 2 μm in width (B) appear uniformly dark since secondary electrons emitted from these hollows have large probability of being absorbed by the specimen.

From the examples shown above it can be deduced that topographic contrast in electron induced and ion induced secondary electron images are similar. This can be predicted since topographic contrast is a result of the effect of the angle of incidence of the primary beam and the angular distribution of the secondary electrons and these two effects have been shown to be similar for both ion and electron bombardment.

Material contrast

As secondary electron yield changes with the nature of the target materials, chemically heterogeneous specimens may exhibit material contrast when the secondary electron yield from different phases on the specimen is sufficiently different. As the ratio between the secondary electron yield of different materials depends also on the nature of the primary species, material contrast for ion and electron induced secondary electron images could be different.

To study material contrast, a tin-zinc alloy with 20% by weight of zinc and a tin-copper alloy with 17% by weight of copper were used as model specimens. The alloys were prepared by first melting mixtures of the pure metals of suitable composition. The molten metals mixtures were heated at 600 °C for 5 hours and then allowed to cool down slowly to encourage phase segregation. A hydrogen atmosphere was maintained in the furnace during the preparation to prevent the formation of oxides. To eliminate topographic effects, the specimens were cut and mechanically polished to obtain a flat surface for examination. Both specimens were examined without further chemical etching.

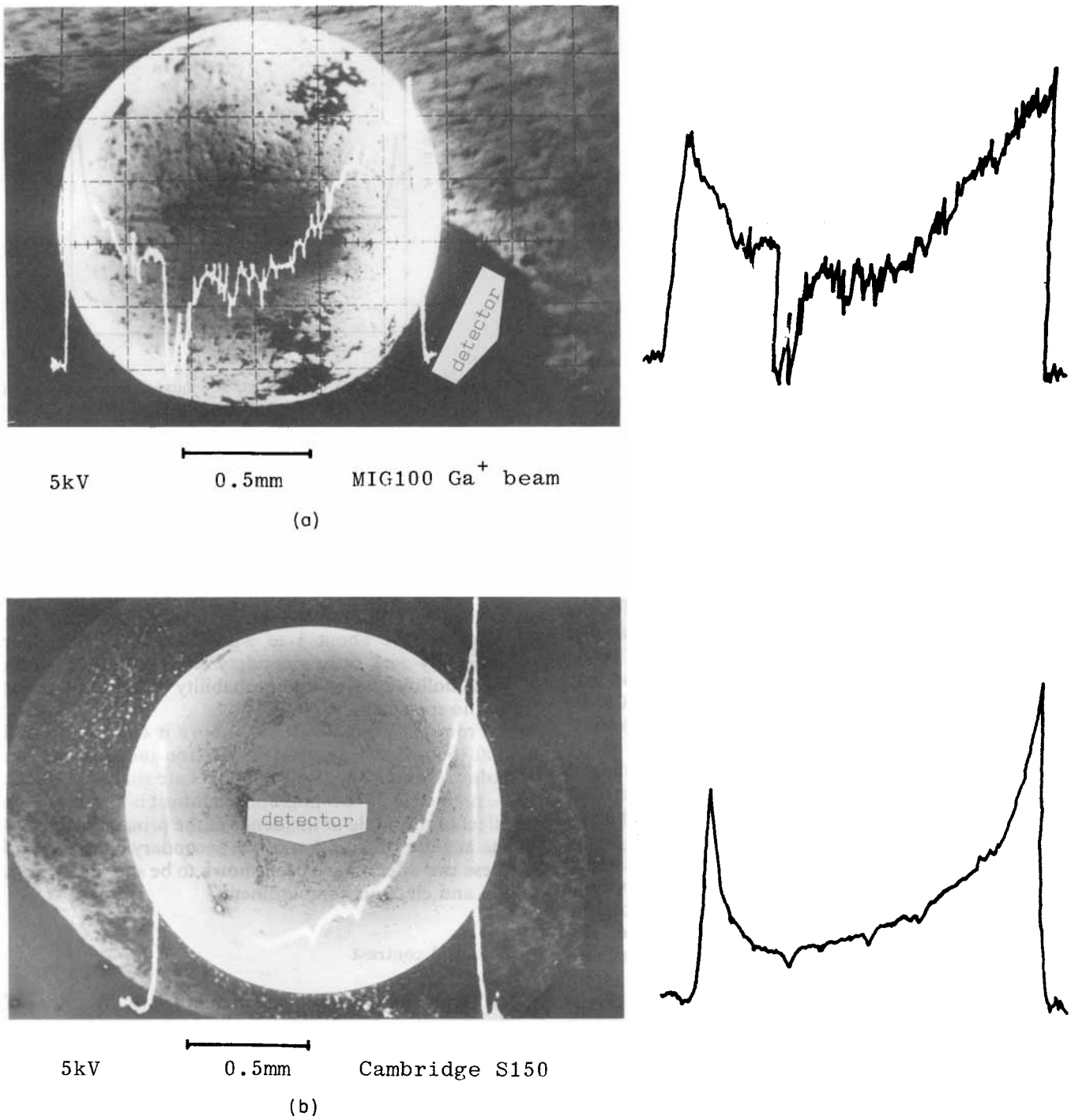

Figure 14. Secondary electron images of a steel sphere. The arrows indicate the position of the electron detectors. For clarity the line scans have been reproduced to almost the same scale alongside each image.

The scanning electron micrographs for the two alloys are shown in Figs 16(a) and (b). Both specimens showed segregation of phases. For the tin-zinc alloy, one observes a dark colour zince-rich phase and a light colour tin-rich matrix. For the tin-copper alloy, three phases were formed. The matrix is a light colour tin-rich phase. Embedded in the matrix is a dark colour copper-rich phase. A phase with intermediate composition was found in the interface of the copper-rich and tin-rich phases and also as scattered particles in the matrix.

After the specimens were sputter cleaned by a 20 μA Ar^+ beam for 2 minutes and then examined with the 10 keV Ga^+ probe, the different phases showed up clearly (Fig. 16(c) and (d)). The contrasts of the Ga^+ induced images and the electron induced images are reversed for both specimens. For the tin-copper specimen, in addition to the material contrast, a crystallographic effect was observed for the copper-rich phase. The grains B and D are oriented in a channelling direction and appear darker than the grains A and C. Despite this complication, the higher coefficient of secondary electron emission from the copper-rich phases compared with the tin-rich matrix is evident. The Ga^+ induced secondary electron images of the two alloys before sputter

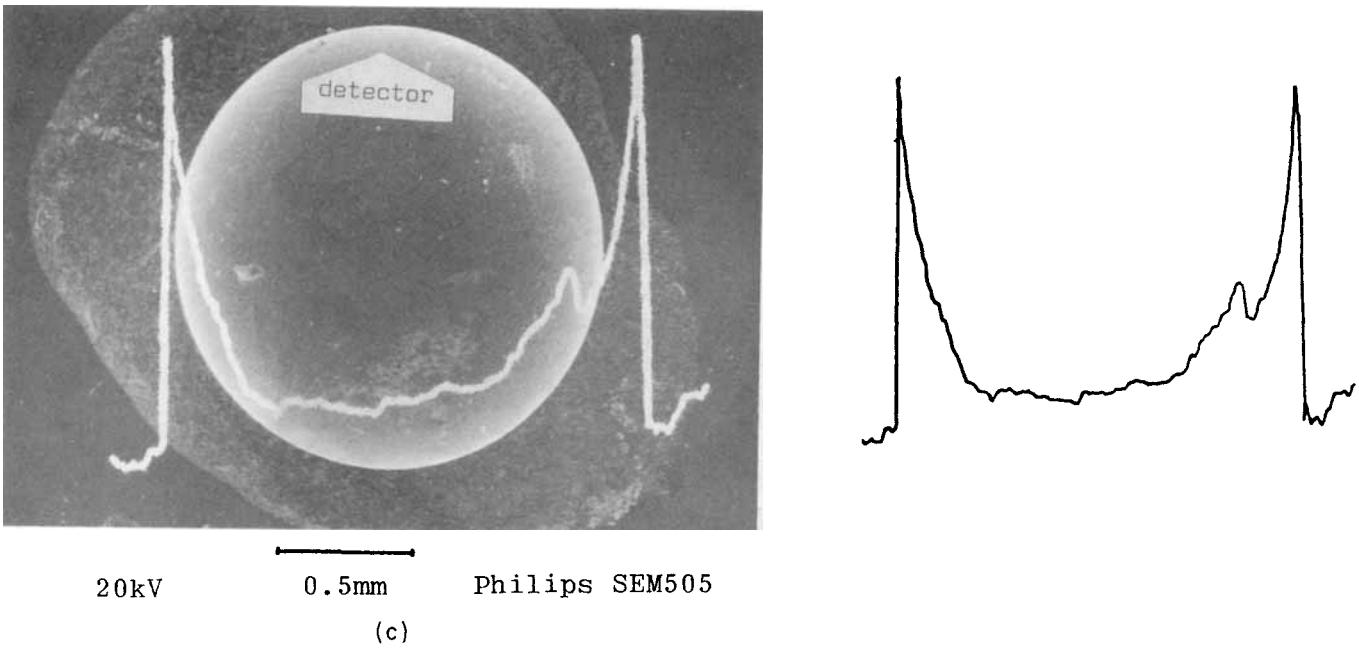

Figure 14. *(cont.)*

cleaning were also shown in Figs 16(e) and (f). For both specimens, the contrasts observed were lower than that obtained after sputter etching. The crystallographic contrast for the copper-rich grains also could not be observed. This is attributed to the presence of a thin layer of oxide on the metal surface which causes a change in the secondary electron yields.

Crystallographic contrast

When polycrystalline specimens are examined, the secondary electron yields from different crystallographic grains depends on the direction of the primary beam with respect to the crystallographic orientation. Grains which are aligned with the primary beam in a direction such that channelling of the primary beam occurs show lower image brightness compared with grains that do not allow channelling.

A polycrystalline brass disc of composition 25% by weight of zinc and 75% by weight of copper was polished and etched with $FeCl_3$/HCl for a few seconds. When examined using 10 keV Ga^+ ion beam without sputter cleaning, the specimen again showed little contrast. After sputter cleaning with a 10 μA Ar^+ beam for 5 minutes, crystallographic contrast becomes clearly observable. As is typical of the crystallographic effect, a small change in the specimen tilt causes a change in the image contrast (Fig. 17). Similar crystallographic contrast effect have also been observed by Levi-Setti *et al.* for the bombardment of copper and silicon with a 60 keV Ga^+ probe.[71,72]

Image information depth

The observations discussed so far suggest that the presence of a thin layer of oxide or other contaminants on the specimen surface have a dramatic effect on the appearance of the secondary electron image produced by Ga^+ ion bombardment but have much less effect for the images produced by electron bombardment. To study this effect, a specimen of silica-alumina and iron pyrite embedded in a plastic matrix and covered with a thin layer of carbon about 20 nm in thickness was examined. The secondary electron images produced by 10 keV electron and Ga^+ ion bombardment are shown in Fig. 18(a) and (b). The material contrast between the mineral particles and the plastic matrix are clearly visible in the electron induced image. In the ion induced image, only the surface topography can be observed. A comparable image was obtained with electron bombardment only when the energy of the primary beam was reduced to 4 keV (Fig. 18(c)). Although it is believed that for both ion and electron bombardment, the true secondary electrons emitted originate only from a thin layer closed to the target surface, in scanning electron microscopy, the information depth can be much larger than the secondary electron escape depth. Since backscattered electrons generate secondary electrons on re-emergence from the specimen, features below the target surface with different coefficients of electron backscattering may be observed.[73] The thickness of the surface layer required to removed the contrast caused by electron backscattering from the underlying layer depends on the difference in the backscattering power of the different elements in the underlying layer. In general, one can assume that if the range of the electron is more than twice the thickness of the surface layer, features in the bulk may be observable.[61,73] In the case of ion bombardment, the effects of the underlying layers on the secondary electron yield of the specimen is not well known. However, a much higher surface sensitivity for ion induced secondary electron imaging compared with that for electron induced secondary electron imaging can be deduced by a simple range comparison. The range of a primary electron beam may be estimated by the experimental universal energy range relationship:[57]

$$\text{Range} = 1.15 \times 10^5 E_0^{1.35}/d$$

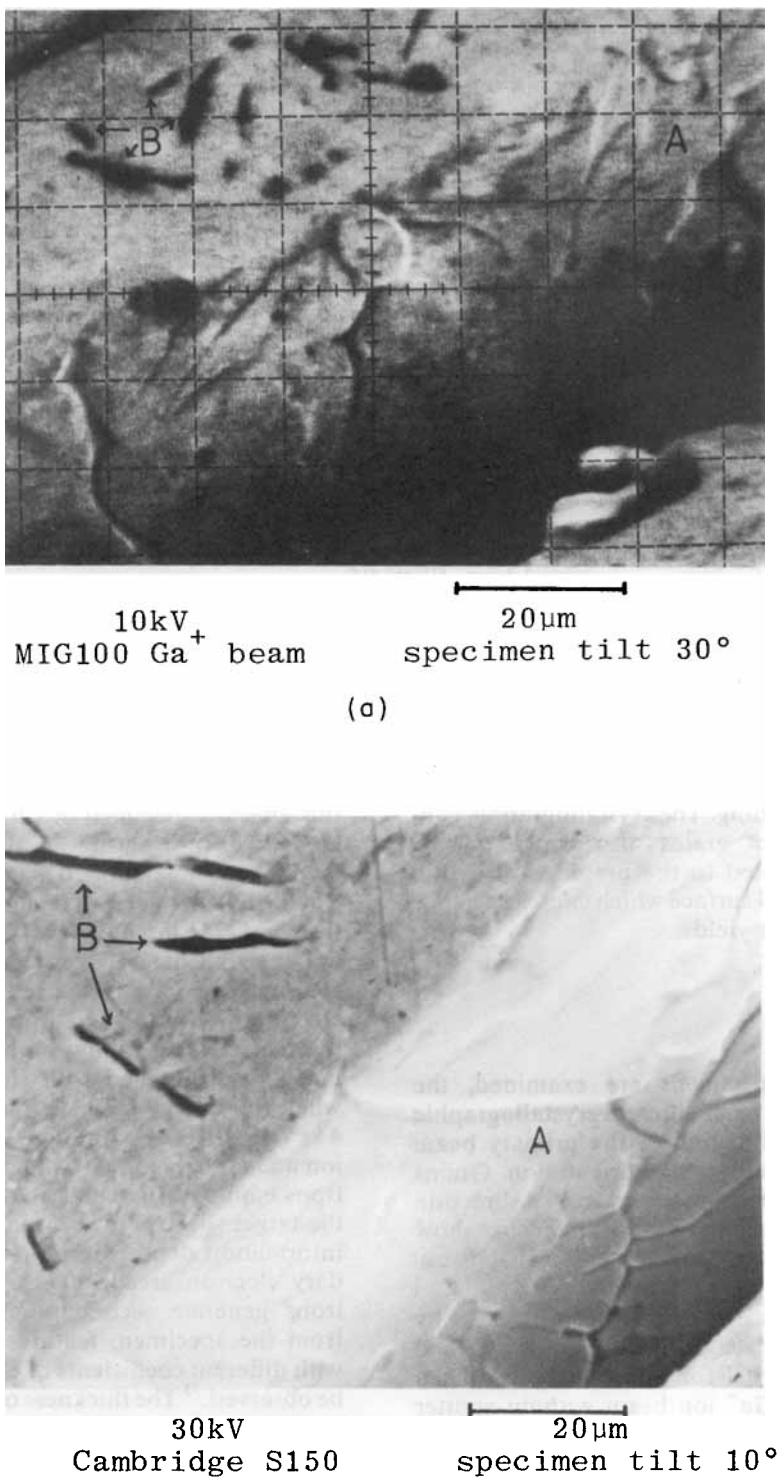

Figure 15. Secondary electron images of a polished Sn–Cu alloy deeply etched with HCl.

where d is the density of the target in kgm^{-3} and the electron range is expressed in units of nm. The range of an ion beam can be estimated if the electronic and nuclear stopping power of the ion-target pair is known. Tabulations of results from theoretical calculations for some ion-target pairs in the keV energy range have been given by Winterbon.[74] No data is given for Ga^+ ion bombardment in this work. However, since in this energy range, energy loss by the ions is mainly by elastic nuclear stopping, which depends on the masses and energies of the colliding species, nickel ion bombardment on carbon may be taken as a suitable model for the present system. According to Winterbon,[74] the range of a 50 kV nickel beam has a range of about 30 nm in carbon, assuming

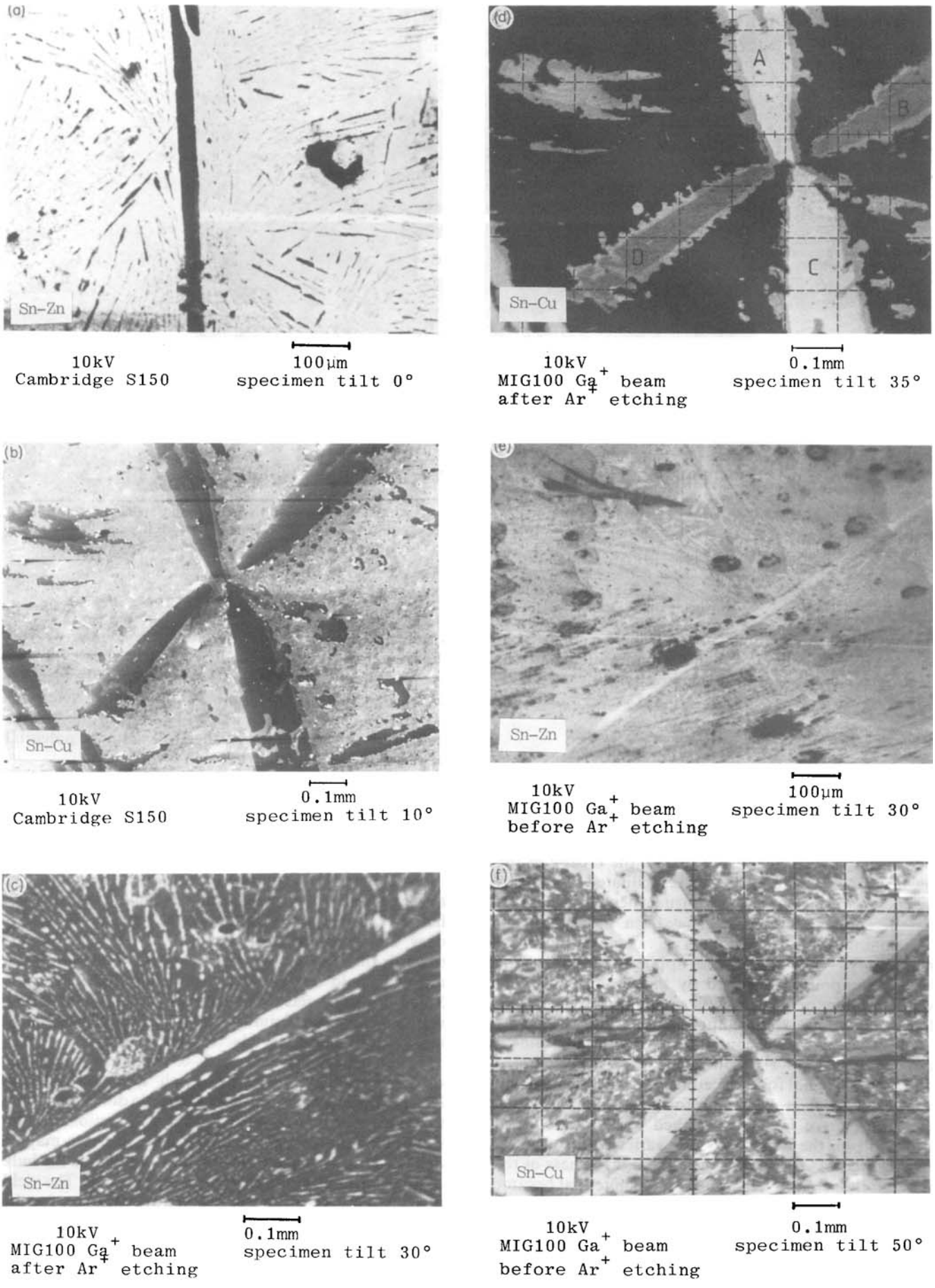

Figure 16. Secondary electron images of polished alloys showing material contrast.

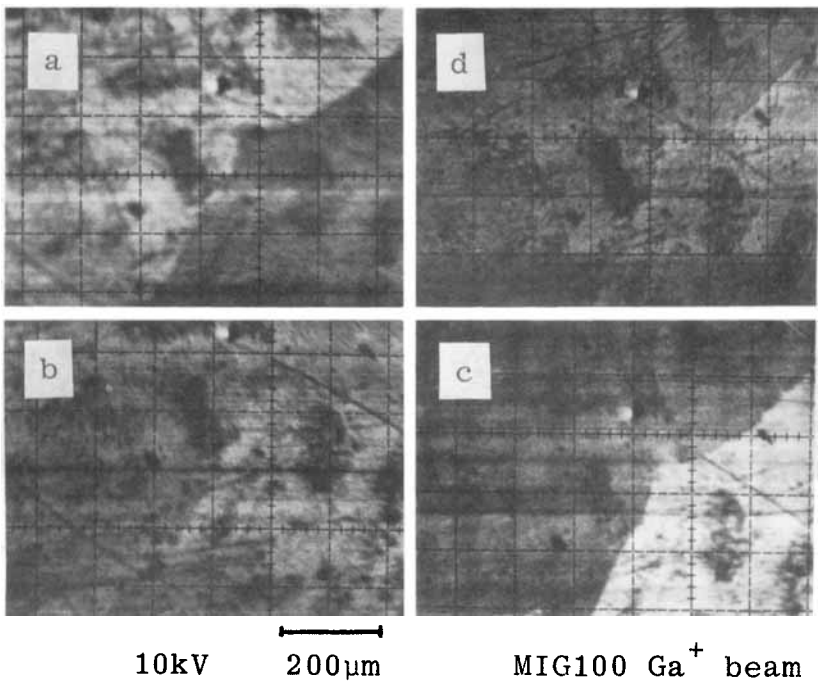

Figure 17. Secondary electron images of a polished brass specimen by 10 keV Ga^+ bombardment with different specimen tilt showing crystallographic contrast; (b) the specimen is tilted 15° relative to (a); (c) the specimen is tilted 30° relative to (a); (d) the specimen is tilted 50° relative to (a).

the density of amorphous carbon to be 2 g cm^{-3}, compared with the value of 1.13×10^4 nm calculated for electron bombardment at the same energy.

Other contrast effects

The contrast features discussed above are those most usually encountered in material studies. In special circumstances, voltage contrast and magnetic contrast may be observed.[69]

If a specimen is negatively biased, the escape of the low energy secondary electrons is facilitated by the surface potential and the reverse is true when it is positively biased. This voltage contrast has been widely used in the examination of microcircuits using scanning electron microscopy. When a voltage is applied to a part of the circuit, components affected by the applied potential will be brighter or darker relative to the rest of the device depending on the voltage applied.

To study voltage contrast in ion bombardment induced secondary electron image, a test specimen of two tantalum metal foils placed side by side but insulated from each other is used. The foil which apears in the left hand side of Fig. 19 is earthed while the potential of the foil on the right hand side varies with the target bias applied. As shown by Fig. 19, the brightness of the biased foil decreases when the surface potential became more positive. When this foil is negatively biased, although the relative signal intensity of this foil compared to the earthed foil has increased compared to when its surface potential is zero, the absolute intensity of the signal has decreased. The local electric field set up between the two metal foils and the quadupole mass spectrometer front end close to the specimen deflects the trajectories of the secondary electrons so that they are not effectively collected by the secondary electron detector. The local field effect is important in determining the image brightness as can be seen in the change in image brightness of the earthed foil when the potential of the other foil is changed.

Another contrast effect that has been observed in scanning electron microscopy is magnetic contrast.[69,75] Magnetic effects have not been studied in our laboratory but its possible effect may be discussed with the knowledge of the emission process.

Type I magnetic contrast occurs when the domain of a magnetic specimen is so arranged that there is a leakage field in the free space outside the specimen. The secondary electrons emitted are deflected away from or towards the detector depending on the direction of the magnetic field relative to the position of the detector. Since this effect acts on the emitted secondary electrons it is expected that a similar effect will be observed with ion-induced secondary electron image.

Type II magnetic contrast is exhibited by specimens of ferromagnetic materials which have no external leakage field but with internal magnetic domains having their magnetic field aligned in different directions. Under suitable conditions, the primary electron beam may be deflected either towards the surface or towards the bulk of the specimen by the internal magnetic field. The yield of backscattered electrons is therefore different for the different magnetic domains. This type of magnetic effect acts on the trajectory of the primary beam. For ion bombardment, the charge state of the primary particles inside the target depend on a balance between the processes of ionization and electron capture. For a

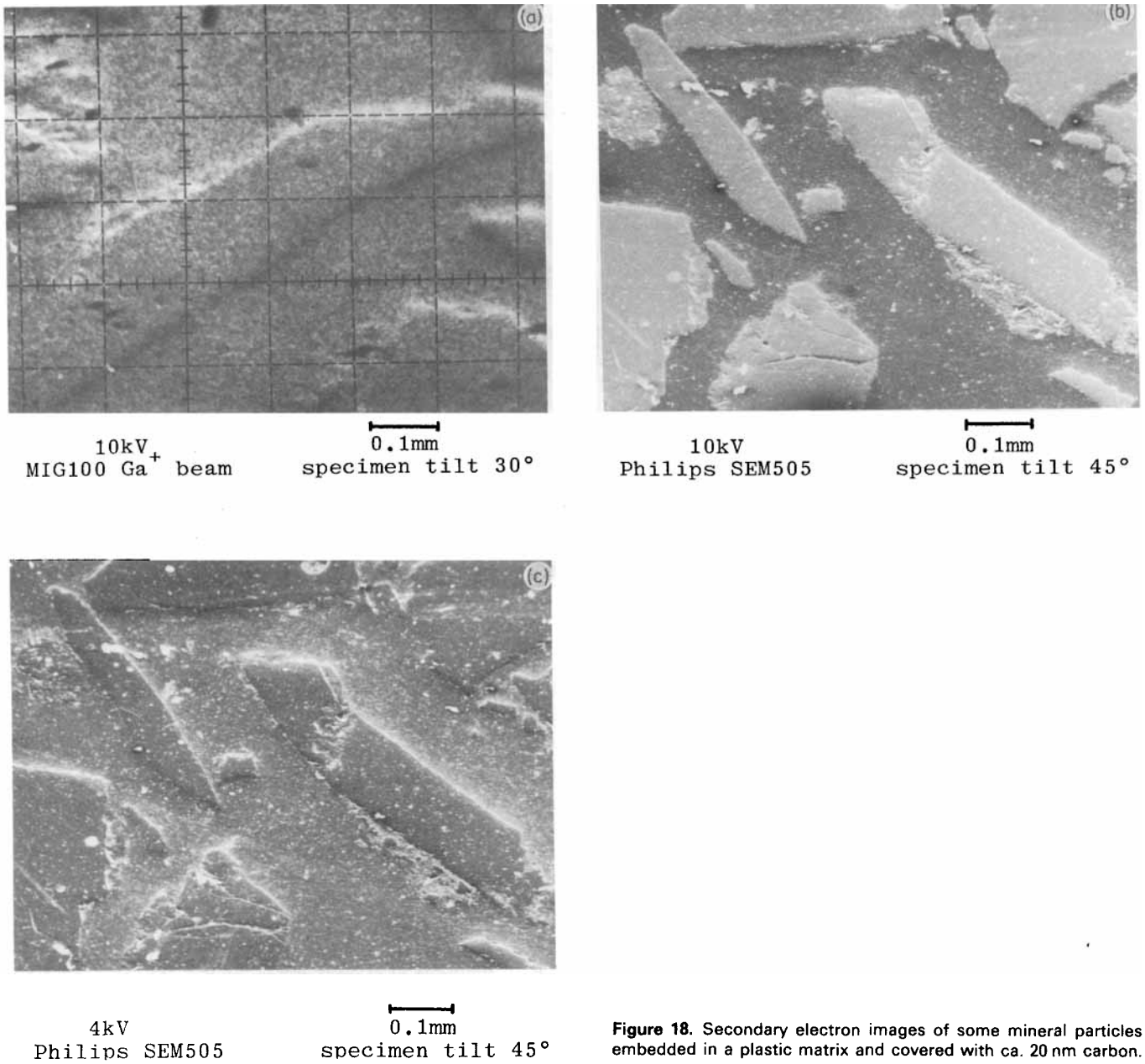

Figure 18. Secondary electron images of some mineral particles embedded in a plastic matrix and covered with ca. 20 nm carbon.

neutralized particle, no deflection can be induced by the magnetic field. Furthermore, since the velocity of an ion beam is much smaller than that of an electron beam of comparable energy, the Lorentz force acting on the primary ions are small. The deflection of the primary ion beam by the internal magnetic field will be negligible and this type of contrast effect will not be expected for ion bombardment.

SUMMARY

It has been shown that the secondary electron images obtained on ion bombardment can yield important information on the topography, material and crystallographic nature of the specimen examined. Many of the contrast mechanisms of ion bombardment induced secondary electron images are qualitatively similar to those for electron bombardment induced secondary electron images in conventional scanning electron microscopy, with the important differences that ion bombardment is the more surface sensitive technique and that material contrast is different for different bombarding species.

Due to the lower spatial resolution achievable for microfocus ion beams compared with microfocus electron beams, it is likely that ion-induced secondary electron imaging will not be used as a tool for routine structural studies in the same way as scanning electron microscopy. However, imaging SIMS holds enormous potential as a form of 'scanning *chemical* microscopy' and since topography, crystallographic structure and surface potential have great influence on the yield of secondary ions on ion bombardment, the knowledge gained from the secondary electron images on these important parameters will be very useful in the correct interpretation of secondary ion images.

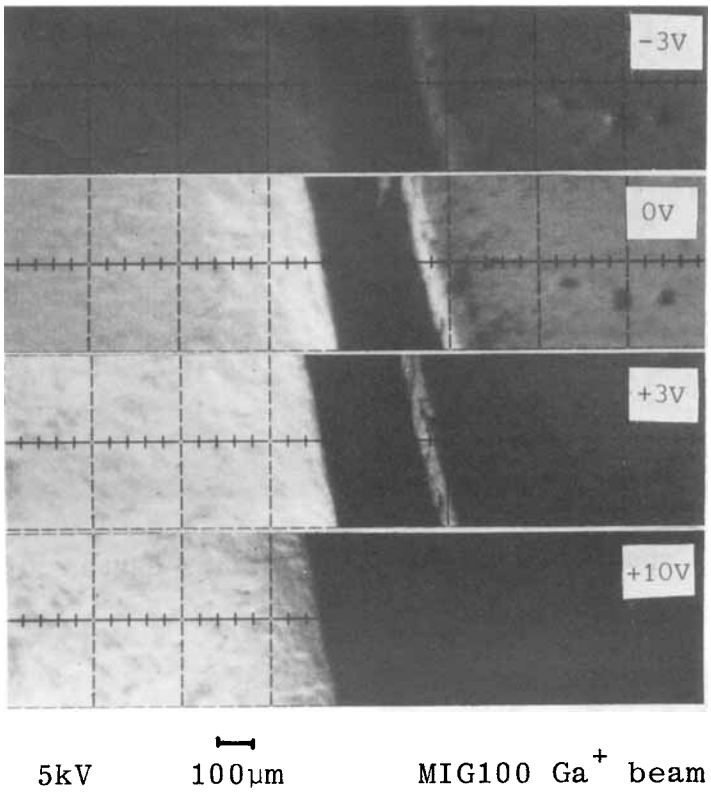

Figure 19. Secondary electron images of two tantalum foils by 5 keV Ga^+ bombardment showing voltage contrast. The foil on the left hand side is earthed and the one on the right hand side is biased at different potentials.

Acknowledgement

The provision of an ICI Joint Research Scheme Award is gratefully acknowledged. The authors also wish to thank Mr. D. Moore of the Corrosion Centre, UMIST and Mr. I. Brough of the Department of Metallurgy, Joint Department of the University of Manchester and UMIST for their help in the work in scanning electron microscopy.

APPENDIX—LIST OF SYMBOLS

e electronic charge
m electronic mass
h Planck's constant
$\hbar$ $h/2\pi$
δ coefficient of secondary electron emission
N number of atoms per unit volume in a target
E_0 energy of a primary ion beam
p collision impact parameter
T energy transfer in an ion-atom or ion-electron collision
u_0 initial velocity of the primary ion beam
u velocity of the primary ion beam at any instant
v_0 Bohr's velocity $= e^2/\hbar$
Z_1 atomic number of the primary ions
Z_2 atomic number of the target atoms
M_1 atomic mass of the primary ions
M_2 atomic mass of the target atoms
a_0 Bohr's radius $= \hbar^2/me^2$
R_0 distance of closest approach between the colliding ion and atoms
ϕ work function of a metal
E_b binding energy of a core level electron
J average energy required for the formation of a secondary electron within the target
P probability for a secondary electron to surmount the surface barrier
x depth within a target
S_e electron stopping power $= -(dE/dx)_{inelastic}$
S_n nuclear stopping power $= -(dE/dx)_{elastic}$
L secondary electron attenuation length

REFERENCES

1. A. R. Bayly, A. R. Waugh and K. Anderson, *Nucl. Inst. Methods Phys. Res.* **218**, 375 (1983).
2. I. A. Abroyan, M. A. Eremeev and N. N. Petrov, *Soviet Physics—Uspekhi* **10**, 332 (1967).
3. I. A. Abroyan, M. A. Eremeev and N. N. Petrov, *Bulletin of the Academy of the USSR—Physical series* **30**, 918 (1966).
4. G. Carter and J. S. Colligon, *Ion Bombardment of Solids.* Heinemann, London (1968).
5. M. Kaminsky, *Atomic and Ionic Impact Phenomena on Metal Surfaces*, Springer-Verlag, Berlin (1965).
6. H. D. Hagstrum, *Phys. Rev.* **96**, 336 (1954).
7. H. D. Hagstrum, in *Inelastic Ion-surface Collision*, ed. by N. H. Tolk *et al.*, pp. 1. Academic Press, New York (1977).
8. R. A. Baragiola, E. V. Alonso, J. Ferron and A. Oliva-Florio, *Surf. Sci.* **90**, 240 (1979).
9. M. Pedrix, J. C. Barboux, R. Goutte and C. Guilland, *J. Phys. D—Appl. Phys.* **3**, 591 (1970).
10. J. Ferron, E. V. Alonso, R. A. Baragiola and A. Oliva-Florio, *Surf. Sci.* **120**, 427 (1982).
11. G. M. Batanov, *Radiotekhnika i Elektronika* **8**, 862 (1963).

12. M. Pedrix, S. Paletto, R. Goutte and C. C. Guilland, *J. Phys. D—Appl. Phys.* **1**, 1517 (1968).
13. M. Perdrix, S. Paletto, R. Goutte and C. Guilland, *Phys. Lett.* **28A**, 534 (1969).
14. M. Perdrix, S. Paletto, R. Goutte and C. Guilland, *J. Phys. D—Appl. Phys*, **2**, 441 (1969).
15. E. R. Cawthron, *Aust. J. Phys* **24**, 859 (1971).
16. R. A. Baragiola, E. V. Alonso and A. Oliva-Florio, *Phys. Rev. B* **19**, 121 (1979).
17. E. V. Alonso, R. A. Baragiola, J. Ferron, M. M. Jakas and A. Oliva-Florio, *Phys. Rev. B* **22**, 80 (1980).
18. J. Ferron, E. V. Alonso, R. A. Baragiola and A. Oliva-Florio, *J. Phys. D—Appl. Phys.* **14**, 1707 (1981).
19. P. C. Zalm and L. J. Becker, *Philips J. Res.* **39**, 61 (1984).
20. B. Svensson, G. Holmen and A. Buren, *Phys. Rev. B* **24**, 3749 (1981).
21. R. F. Pottie, D. L. Cocke and K. A. Gingerich, *Int. J. Mass Spectrometry Ion Phys.* **11**, 41 (1973).
22. U. Fehn, *Int. J. Mass Spectrometry Ion Phys*, **21**, 1 (1976).
23. F. Thum and W. O. Hofer, *Nucl. Inst. Methods Physl Res. B* **2**, 531 (1984).
24. Z. Seiler, *Z. Angew. Phys.* **22**, 249 (1966).
25. L. Viel, C. Benazeth and N. Benazeth, *Surf. Sci.* **54**, 635 (1976).
26. D. Hasselkamp and A. Scharmann, *Surf. Sci.* **119**, L388 (1982).
27. G. Wehner, *Z. Physik* **193**, 439 (1966).
28. R. C. Abbot and H. W. Berry, *J. Appl. Phys.* **30**, 871 (1959).
29. J. Mischler, N. Benazeth, M. Negre and C. Benazeth, *Surf. Sci.* **136**, 532 (1984).
30. E. Veje, *Nucl. Inst. Methods Phys. Res. B* **2**, 536 (1984).
31. V. Evdokimo, E. S. Mashkova and V. A. Molchanov, *Phys. Lett.* **25A**, 619 (1967).
32. I. A. Abroyan, *Soviet Physics—Solid State* **3**, 431 (1961).
33. N. N. Petrov, *Soviet Physics—Solid State* **2**, 857 (1960).
34. E. J. Sternglass and M. M. Wachtel, *Phys. Rev.* **99**, 464 (1955).
35. C. E. Carlston, G. D. Magnuson, P. Mahadevan and D. E. Harrison, *Phys. Rev.* **139**, A729 (1965).
36. I. N. Evdokimov, V. A. Molchanov, D. D. Odintsov and V. M. Chickerov, *Soviet Phys.—Solid State* **8**, 2348 (1967).
37. U. Von Gemmingen, *Surf. Sci.* **120**, 334 (1982).
38. J. Linhard and M. Scharff, *Phys. Rev.* **124**, 128 (1961).
39. Ya. A. Teplova, V. S. Nikolaev and I. S. Dmitriev, *Soviet Physics—JETP* **15**, 31 (1962).
40. N. Bohr, *Dan. Vid. Selsk. Mat. Fys. Medd.* **18**, no. 8 (1948).
41. H. A. Bethe, *Ann. Physik* **5**, 325 (1930).
42. O. B. Firsov, *Soviet Physics—JETP* **36**, 1076 (1959).
43. E. S. Parilis and L. M. Kishinevskii, *Soviet Physics—Solid State* **3**, 885 (1960).
44. L. M. Kishinevskii and E. S. Parilis, *Bulletin of the Academy of Science of the USSR: Physical Series* **26**, 1409 (1962).
45. Ya. A. Vinokurov, L. M. Kishinevskii and E. S. Parilis, *Bulletin of the Academy of Science of the USSR: Physical Series* **40**, 166 (1976).
46. D. E. Harrison, C. E. Carlston and G. D. Magnuson, *Phys. Rev.* **139**, A737 (1965).
47. E. J. Sternglass, *Phys. Rev.* **108**, 1 (1957).
48. J. Schou, *Phys. Rev. B* **22**, 2141 (1980).
49. J. Schou, *Nucl. Inst. Methods Phys. Res.* **170**, 317 (1980).
50. G. Holmen, B. Svensson, J. Schou and P. Sigmund, *Phys. Rev. B* **20**, 2247 (1979).
51. Yu. V. Martynenko in *Atomic Collision Phenomena in Solids*, ed. by D. W. Palmer, M. W. Thompson and P. D. Townsend, pp. 440–416. North-Holland (1970).
52. G. Carter and W. A. Grant, *ion Implantation of Semiconductors*, Edward Arnold (1976).
53. R. S. Nelson, and M. W. Thompson, *Phil. Mag.* **8**, 1677 (1963).
54. J. Linhard, *Dan. Vid. Selsk. Mat. Fys. Medd.* **34**, no. 14 (1965).
55. A. J. Dekker, *Solid State Physics* **6**, 251 (1958).
56. O. Hachenberg and W. Bauer, *Adv. Electron. Electron Phys.* **11**, 413 (1959).
57. H. Seiler in *Electron Beam Interactions with Solids*, ed. by D. F. Kyser, D. E. Newbury, H. Niedrig, and R. Shimuzu, pp. 33–42. SEM Inc., Chicago (1984).
58. T. E. Everhart, N. Saeki, R. Shimuzu and T. Koshikawa, *J. Appl. Phys.* **47**, 2941 (1976).
59. H. Jahrreiss and W. Oppel, *J. Vacuum Sci. Techn.* **9**, 173 (1972).
60. G. F. Rouse in *Amer. Inst. Phys. Handbook*, pp. 158–160. McGraw-Hill, New York (1957).
61. J. E. Holliday and E. F. Sternglass, *J. Appl. Phys.* **28**, 1189 (1957).
62. T. E. Everhart, *J. Appl. Phys.* **31**, 1483 (1960).
63. H. Salow, *Z. Physik* **41**, 434–442 (1940).
64. H. Bruining, *Physics and Applications of Secondary Electron Emission*, Pergamon, London (1954).
65. J. R. Young, *J. Appl. Phys.* **27**, 1 (1956).
66. J. R. Young, *J. Appl. Phys.* **28**, 524 (1956).
67. K. Kanaya and H. Kawakatsu, *J. Phys. D.—Appl. Phys.* **5**, 1727 (1977).
68. D. E. Newbury in *Practical Scanning Electron Microscopy*, ed. by J. I. Goldstein and H. Yakowitz, Chapter 4, pp. 95–148. Plenum, New York, (1975).
69. D. E. Newbury and H. Yakowitz in *Practical Scanning Electron Microscopy*, ed. by J. I. Goldstein and H. Yakowitz, Chapter 5, pp. 149–210. Plenum, New York, (1975).
70. A. Brown and J. C. Vickerman, *Analyst* **109**, 851 (1984).
71. R. Levi-Setti, P. H. La Marche, K. Lam, T. H. Shields and Y. Wang, *Nucl. Inst. Methods Phys. Res.* **218**, 368 (1983).
72. P. H. La Marche, R. Levi-Setti and K. Lam, *IEEE Trans. Nucl. Sci.* **NS-30**, 1240 (1983).
73. O. C. Wells, R. J. Savoy and P. J. Bailey in *Electron Beam Interaction with Solids*, ed. by D. F. Kyser, D. E. Newbury, H. Niedrig and R. Shimuzu, pp. 287–298. SEM Inc., Chicago (1984).
74. K. B. Winterbon, *Ion Implantation Range and Energy Deposition distributions vol. 2—Low incident Ion Energies*, Plenum, New York (1975).
75. L. J. Balk and J. B. Elsbrock in *Scanning Electron Microsc.* **I: 141**, (1984).